OXFORD GENETICS

GENETICS, 2023, 224(4), iyad061
https://doi.org/10.1093/genetics/iyad061
Advance Access Publication Date: 10 April 2023
Genetic Models of Rare Diseases

Genetic and genomic analyses of *Drosophila melanogaster* models of chromatin modification disorders

Rebecca A. MacPherson, Vijay Shankar, Robert R.H. Anholt ,* Trudy F.C. Mackay*

Center for Human Genetics and Department of Genetics and Biochemistry, Clemson University, 114 Gregor Mendel Circle, Greenwood, SC 29646, USA

*Corresponding author: Email: ranholt@clemson.edu; tmackay@clemson.edu

Abstract

Switch/sucrose nonfermentable (SWI/SNF)-related intellectual disability disorders (SSRIDDs) and Cornelia de Lange syndrome are rare syndromic neurodevelopmental disorders with overlapping clinical phenotypes. SSRIDDs are associated with the BAF (*Brahma-Related Gene-1* associated factor) complex, whereas CdLS is a disorder of chromatin modification associated with the cohesin complex. Here, we used RNA interference in *Drosophila melanogaster* to reduce the expression of six genes (*brm*, *osa*, *Snr1*, *SMC1*, *SMC3*, *vtd*) orthologous to human genes associated with SSRIDDs and CdLS. These fly models exhibit changes in sleep, activity, startle behavior (a proxy for sensorimotor integration), and brain morphology. Whole genome RNA sequencing identified 9,657 differentially expressed genes (FDR < 0.05), 156 of which are differentially expressed in both sexes in SSRIDD- and CdLS-specific analyses, including *Bap60*, which is orthologous to *SMARCD1*, an SSRIDD-associated BAF component. k-means clustering reveals genes co-regulated within and across SSRIDD and CdLS fly models. RNAi-mediated reduction of expression of six genes co-regulated with focal genes *brm*, *osa*, and/or *Snr1* recapitulated changes in the behavior of the focal genes. Based on the assumption that fundamental biological processes are evolutionarily conserved, Drosophila models can be used to understand underlying molecular effects of variants in chromatin-modification pathways and may aid in the discovery of drugs that ameliorate deleterious phenotypic effects.

Keywords: Coffin–Siris syndrome, Nicolaides–Baraitser syndrome, SWI/SNF-related intellectual disability disorders, Cornelia de Lange syndrome, RNAi, RNA sequencing

Introduction

Switch/sucrose nonfermenting (SWI/SNF)-related intellectual disability disorders (SSRIDDs) and Cornelia de Lange syndrome (CdLS) are syndromic neurodevelopmental Mendelian disorders of chromatin modification. SSRIDDs, including Coffin–Siris syndrome (CSS) and Nicolaides–Baraitser syndrome (NCBRS), stem from variants in genes of the *Brahma-Related Gene-1* Associated Factor (BAF) complex, also known as the mammalian SWI/SNF complex (Hoyer *et al.* 2012; Santen *et al.* 2012; Tsurusaki *et al.* 2012; Van Houdt *et al.* 2012; Tsurusaki *et al.* 2014; Hempel *et al.* 2016; Bramswig *et al.* 2017; Bogershausen and Wollnik 2018; Vasileiou *et al.* 2018; Gazdagh *et al.* 2019; Machol *et al.* 2019; Zawerton *et al.* 2019). CdLS is associated with variants in genes that encode components of the cohesin complex (Krantz *et al.* 2004; Deardorff *et al.* 2007; Deardorff *et al.* 2012; Gil-Rodriguez et al. 2015; Boyle *et al.* 2017; Huisman *et al.* 2017; Olley *et al.* 2018).

SSRIDD patients exhibit neurodevelopmental delay, intellectual disability, hypotonia, seizures, and sparse hair growth, as well as a cardiac, digit, and craniofacial anomalies, where the severity and spectrum of affected phenotypes are dependent upon the specific variant or affected gene product (reviewed in Schrier Vergano *et al.* 2013; Bogershausen and Wollnik 2018; Vasko *et al.* 2021). For example, many SSRIDD patients with variants in *ARID1B* tend to have milder phenotypes including normal growth, milder facial gestalt, and no central nervous system (CNS) abnormalities, whereas most variants in *SMARCB1* are associated with more severe phenotypes, including profoundly delayed developmental milestones, seizures, kidney malformations, and CNS abnormalities (Schrier Vergano *et al.* 2013; Bogershausen and Wollnik 2018). Furthermore, variants in *ARID1B* are associated with SSRIDD, Autism Spectrum disorder, and nonsyndromic intellectual disability (Hoyer *et al.* 2012; De Rubeis *et al.* 2014; Iossifov *et al.* 2014; Vissers *et al.* 2016; van der Sluijs *et al.* 2019). Brain malformations, such as agenesis of the corpus callosum, Dandy–Walker malformation, and cerebellar hypoplasia, have also been observed in 20–30% of all patients with variants in the BAF complex (Vasko and Schrier Vergano 2022), but are most commonly observed in patients with variants in *SMARCB1* (Bogershausen and Wollnik 2018).

CdLS patients also display a clinical spectrum including intellectual disability, hirsutism, synophrys, and digit, craniofacial, and CNS anomalies (reviewed in Kline *et al.* 2018; Avagliano *et al.* 2020; Selicorni *et al.* 2021). As in SSRIDDs, some phenotypes are more highly associated with a specific gene, but phenotypic severity can vary widely across variants within the same gene. For example, most patients with variants in *SMC1A* show milder developmental delay and intellectual disability compared to their classical *NIPBL*-CdLS counterparts, but about 40% of *SMC1A* patients exhibit severe epileptic encephalopathy and intellectual disability (Jansen *et al.* 2016; Symonds *et al.* 2017; Selicorni *et al.* 2021).CdLS has also been reclassified as a spectrum of

Received: November 10, 2022. **Accepted:** March 30, 2023

cohesinopathies (Van Allen *et al.* 1993; Kline *et al.* 2018). Patients with pathogenic variants in many genes involved in chromatin accessibility and regulation have overlapping symptoms with CdLS (Parenti *et al.* 2017; Aoi *et al.* 2019; Cucco *et al.* 2020).

D. melanogaster is well-suited for modeling human disorders, as large numbers of flies can be raised economically without ethical or regulatory restrictions. Additionally, SSRIDD- and CdLS-associated genes are highly conserved in flies and a wide variety of genetic tools are available to create fly models of human diseases (Hu *et al.* 2011; Perkins *et al.* 2015; Zirin *et al.* 2020). Previous groups have used *D. melanogaster* to investigate SSRIDDs and CdLS and have observed phenotypes relevant to disease presentation in humans, including changes in sleep, brain function, and brain morphology (Pauli *et al.* 2008; Schuldiner *et al.* 2008; Wu *et al.* 2015; Chubak *et al.* 2019). These studies have provided insight into potential disease pathogenesis and suggested that certain subtypes of SSRIDD and CdLS can be modeled on the fly, but they were not performed in controlled genetic backgrounds.

Here, we present behavioral and transcriptomic data on Drosophila models of SSRIDDs and CdLS in a common genetic background. RNAi-mediated knockdown of Drosophila orthologs of SSRIDD- and CdLS-associated genes show gene- and sex-specific changes in brain structure and sensorimotor integration, as well as increased locomotor activity and decreased night sleep. Transcriptomic analyses show distinct differential gene expression profiles for each focal gene.

Materials and methods

Drosophila genes and stocks

We selected SSRIDD- and CdLS-associated genes with a strong fly ortholog (*Drosophila* RNAi screening center integrative ortholog prediction tool (DIOPT) score >9) (Hu *et al.* 2011) and a corresponding *attp2* fly line available from the transgenic RNAi project (TRiP) (Perkins *et al.* 2015; Zirin *et al.* 2020). We excluded human genes that were orthologous to multiple fly genes to increase the likelihood of aberrant phenotypes upon knockdown of a single fly ortholog. We used *attp40* TRiP lines when assessing phenotypes associated with the knockdown of co-regulated genes. We used the y^1, sc^*, v^1, sev^{21}; *TRiP2; TRiP3* genotypes as the control *UAS* line in all experiments. With the exception of the initial viability screen, we crossed all RNAi lines to a weak ubiquitous *GAL4* driver line, *Ubi156-GAL4* (Garlapow *et al.* 2015). Supplementary Table 1a lists the Drosophila stocks used.

Drosophila culture

For all experiments, we maintained flies at a controlled density on standard cornmeal/molasses medium (Genesee Scientific, El Cajon, CA) supplemented with yeast in controlled environmental conditions (25°C, 50% relative humidity, 12-hour light-dark cycle (lights on at 6 AM)). Crosses contained five flies of each sex, with fresh food every 48 hours. After eclosion, we aged flies in mixed-sex vials at a density of 20 flies per vial until used in experiments. We performed experiments on 3–5-day old flies from 8 AM to 11 AM unless otherwise noted.

Viability

For the initial viability screen of Drosophila orthologs of SSRIDD- and CdLS-associated genes, we crossed *attp2* TRiP lines and the control line to three ubiquitous *GAL4* driver lines. For the viability screen of co-regulated genes, we crossed *attp40* TRiP lines and the control line to the *Ubi156-Gal4* driver line. From days 0–15, we noted the developmental stage. For stocks that contained balancers, we recorded the associated phenotypic marker in eclosed progeny.

Quantitative real-time PCR (qRT-PCR)

For the qRT-PCR analyses of gene expression of RNAi targets of *brm*, *osa*, *SMC1*, *SMC3*, *Snr1*, and *vtd*, we flash froze 3–5-day old whole flies on dry ice and then collected, sexes separately, 30 flies per sample. We stored frozen flies and their extracted RNA at −80°C. We extracted RNA using the Qiagen RNeasy Plus Mini Kit (Qiagen, Hilden, Germany) by homogenizing tissue with 350 μL of RLT Plus Buffer containing β-mercaptoethanol (Qiagen) and DX reagent (Qiagen), using a bead mill at 5 m/second for 2 minutes. We quantified RNA with the Qubit RNA BR Assay Kit (ThermoFisher Scientific, Waltham, MA) on a Qubit Fluorometer (ThermoFisher Scientific) according to the manufacturer's specifications. We synthesized cDNA using iScript Reverse Transcription Supermix (Bio-Rad Laboratories, Inc., Hercules, CA) according to the manufacturer's instructions. We quantified expression using quantitative real-time PCR with SYBR™ Green PCR Master Mix (ThermoFisher Scientific), according to manufacturer specifications, but with a total reaction volume of 20μL. We used three biological and three technical replicates per sample and calculated percent knockdown using the ΔΔ*ct* method (Livak and Schmittgen 2001). Supplementary Table 1b contains the primer sequences used. For the qRT-PCR analyses of gene expression for the co-regulated genes *Alp10*, *CG40485*, *CG5877*, *IntS12*, *Mal-A4*, and *Odc1*, we extracted RNA using the Direct-zol RNA MiniPrep Plus Kit (Zymo Research, Irvine, CA) and homogenized tissue with 350 μL of Tri-Reagent, using a bead mill at 5 m/second for 2 minutes. We used two technical replicates in the qRT-PCR analyses of co-regulated genes.

Startle-Induced locomotor response

We assessed startle response using a variation of a previously described assay (Yamamoto *et al.* 2008). In summary, 36–50 flies per sex per line were placed into individual vials to acclimate 24 hours before testing. To standardize the mechanical startle stimulus, we placed a vial housing a single 3–5-day old fly in a chute. Removal of a supporting dowel allows the vial to drop from a height of 42 cm, after which it comes to rest horizontally (Huggett *et al.* 2021). We measured the total time the fly spent moving during a period of 45 s immediately following the drop. We also recorded whether the fly demonstrated a tapping phenotype, a series of leg extensions without forward movement. Time spent tapping was not considered movement for startle calculations.

Sleep and activity

We used the Drosophila Activity Monitoring System (DAM System, TriKinetics, Waltham, MA) to assess sleep and activity phenotypes. At 1–2 days of age, we placed flies into DAM tubes containing 2% agar with 5% sucrose, sealed with a rubber cap (TriKinetics), and a small piece of yarn. We collected data for 7 days on a 12-hour light-dark cycle, with sleep defined as at least 5 minutes of inactivity. We discarded data from flies that did not survive the entire testing period, leaving 18–32 flies per sex per line for analysis. We processed the raw sleep and activity data using ShinyR-DAM (Cichewicz and Hirsh 2018) and used the resulting output data for statistical analysis.

Dissection and staining of brains

We dissected brains from cold-anesthetized flies in cold phosphate buffered saline (PBS), before we fixed the brains with 4% paraformaldehyde (v/v in PBS) for 15 minutes, washed with

PAXD buffer (1× PBS, 0.24% (v/v) Triton-X 100, 0.24% (m/v) sodium deoxycholate, and 5% (m/v) bovine serum albumin) three times for 10 minutes each, and then washed three times with PBS. We blocked fixed brains with 5% Normal Goat Serum (ThermoFisher Scientific; in PAXD) for 1 hour with gentle agitation, then stained with 2–5 μg/mL of Mouse anti-Drosophila 1D4 anti-Fasciclin II (1:4) (Developmental Studies Hybridoma Bank; Iowa City, IA) for 16–20 hours at 4°C. We washed brains three times with PAXD for 10 minutes and stained them with Goat anti-Mouse IgG-AlexaFluor488 (1:100) (Jackson ImmunoResearch Laboratories, Inc., West Grove, PA) for 4 hours. Then, we washed brains with PAXD three times for 10 minutes each before mounting with ProLong Gold (ThermoFisher Scientific). We performed all steps at room temperature with gentle agitation during incubations.

Brain measurements

We analyzed 17–20 brains per sex per line using a Leica TCS SPE confocal microscope. We visualized the Z-stacks of each brain using Icy v. 2.2.0.0 (de Chaumont *et al.* 2012).

We measured ellipsoid body height and ellipsoid body width by measuring vertical ellipsoid body length from dorsal to ventral, and horizontal ellipsoid body length from left to right (relative to the fly). We also measured the lengths of the mushroom body alpha and beta lobes by drawing a single 3D line (3DPolyLine Tool within Icy) through the center of each lobe, adjusting the position of the line while progressing through the z-stack. We measured alpha lobes from the dorsal end of the alpha lobe to the alpha/beta lobe heel (where the alpha and beta lobes overlap) and beta lobes from the median end of the beta lobe to the alpha/beta lobe heel. We normalized the measurements for each brain using the distance between the left and right heels of the mushroom body (heel-heel distance). We used the average alpha and beta lobe lengths for each brain for subsequent analyses. In the case of one missing alpha or beta lobe, we did not calculate an average and instead, used the length of the remaining lobe for analysis. If both alpha or both beta lobes were missing, we removed that brain for analysis of the missing lobes but retained it for analysis of the other brain regions.

We also recorded gross morphological abnormalities of the mushroom body alpha and beta lobes, including missing lobe, skinny lobe, extra projections, abnormal alpha lobe outgrowth, and beta lobes crossing the midline for each brain. We selected these phenotypes based on prior studies on gross mushroom body morphology (Zwarts *et al.* 2015; Chubak *et al.* 2019).

Statistical analyses

Unless noted below, we analyzed all behavioral data and brain morphology data in SAS v3.8 (SAS Institute, Cary, NC) using the "PROC GLM" command according to the Type III fixed effects factorial ANOVA model $Y = \mu + L + S + L \times S + \varepsilon$, where Y is the phenotype, μ is the true mean, L is the effect of a line (e.g. RNAi line vs the control), S is the effect of sex (males, females), and ε is residual error. We performed comparisons between an RNAi line and its control. We also performed additional analyses for each sex separately.

We used Fisher's exact test (*fisher.test* in R v3.63) to analyze the proportion of flies tapping during startle experiments, the number of brains with a specific morphological abnormality, and the number of brains with any gross morphological abnormality.

We performed Levene's and Brown-Forsythe's Tests for unequal variances on the same data set used for the analysis of lobe lengths. For both tests, we used the *leveneTest* command ((*car* v3.0-11, Fox and Sanford 2019) in R v3.6.3) to run a global analysis comparing all genotypes as well as pairwise comparisons.

RNA sequencing

We synthesized libraries from 100 ng of total RNA using the Universal RNA-seq with Nuquant + UDI kit (Tecan Genomics, Inc., CA) according to manufacturer recommendations. We converted RNA into cDNA using the integrated DNase treatment and used the Covaris ME220 Focused-ultrasonicator (Covaris, Woburn, MA) to generate 350 bp fragments. We performed ribosomal RNA depletion and bead selection using Drosophila AnyDeplete probes and RNAClean XP beads (Beckman Coulter, Brea, CA), respectively. We purified libraries after 17 cycles of PCR amplification. We measured library fragment sizes on the Agilent Tapestation using the Agilent High Sensitivity DNA 1000 kit (Agilent Technologies) and quantified library concentration using the Qubit 1X dsDNA High Sensitivity Assay kit (Thermo Fisher Scientific). We pooled libraries at 4 nM and loaded them onto an Illumina S1 flow cell (Illumina, Inc., San Diego, CA) for paired-end sequencing on a NovaSeq6000 (Illumina, Inc., San Diego, CA). We sequenced three biological replicates of pools of 30 flies each per sex per line. We sequenced each sample to a depth of ~30 million total reads; we resequenced samples with low read depth (<8 million uniquely mapped reads).

We used the default Illumina BaseSpace NovaSeq sequencing pipeline to demultiplex the barcoded sequencing reads. We then merged S1 flow cell lanes, as well as reads from different runs. We filtered out short and low-quality reads using the *AfterQC* pipeline (v0.9.7) (Chen *et al.* 2017) and quantified the remaining levels of rRNA via the bbduk command (Bushnell 2014). We aligned reads to the reference genome (*D. melanogaster* v6.13) using GMAP-GSNAP (Wu *et al.* 2016) and counted these unique alignments to Drosophila genes using the feature counts pipeline from the Subread package (Liao *et al.* 2013). We excluded genes with a median expression across all samples of less than 3 and genes where greater than 25% of the samples had a count value of 0. We then normalized the data based on gene length and library size using Ge-TMM (Smid *et al.* 2018) before differential expression analysis.

Differential expression analyses

We performed multiple analyses for differential expression in SAS (v3.8; Cary, NC) using the "PROC glm" command. We first performed a fixed effects factorial ANOVA model $Y = \mu + L + S + L \times S + \varepsilon$, where Line ($L$, all RNAi and control genotypes) and Sex (S) are cross-classified main effects and Line × Sex ($L \times S$) is the interaction term, Y is gene expression, μ is the overall mean, and ε is residual error. We then performed the same analyses only for genes associated with SSRIDDs or for CdLS; i.e. 9,657 genes that were significantly differentially expressed (FDR < 0.05 for the line and/or line × sex terms) in the full model. We ran the ANOVA model for each RNAi genotype compared to the control. Finally, we ran ANOVAs ($Y = \mu + L + \varepsilon$) separately for males and females for the disease-specific and individual RNAi analyses.

Gene ontology and k-means clustering analyses

We performed Gene Ontology (GO) statistical over-representation analyses on the top 1,000 differentially expressed genes for the Line term (GO Ontology database released 2022 March 22, Pantherdb v16.0 (Mi *et al.* 2013; Thomas *et al.* 2022)) in each disease-specific and pairwise analysis for GO biological process, molecular function, and reactome pathway terms. For the analyses performed on sexes separately, we used the top 600

Table 1. Drosophila genes used in fly models.

Fly Gene	Human Ortholog(s)	Human Ortholog MIM Number(s)	Associated Human Disease	Phenotype MIM Number(s)	DIOPT Score
brm	*SMARCA2, SMARCA4*	600014, 603254	SSRIDD (NCBRS, CSS4)	601358, 614609	13, 12
osa	*ARID1A, ARID1B*	603024, 614556	SSRIDD (CSS2, CSS1)	614607, 135900	12, 12
SMC1	*SMC1A*	300040	Cornelia de Lange syndrome 2	300590	12
SMC3	*SMC3*	606062	Cornelia de Lange syndrome 3	610759	12
Snr1	*SMARCB1*	601607	SSRIDD (CSS3)	614608	15
vtd	*RAD21, RAD21L1*	606462, 619533	Cornelia de Lange syndrome 4	614701	11, 10

The table indicates fly genes used in SSRIDD and CdLS fly models, as well as the respective human orthologs and MIM numbers, associated human disease and respective MIM numbers, and DIOPT scores. Human orthologs are only included in the table if the DIOPT score is greater than 9.

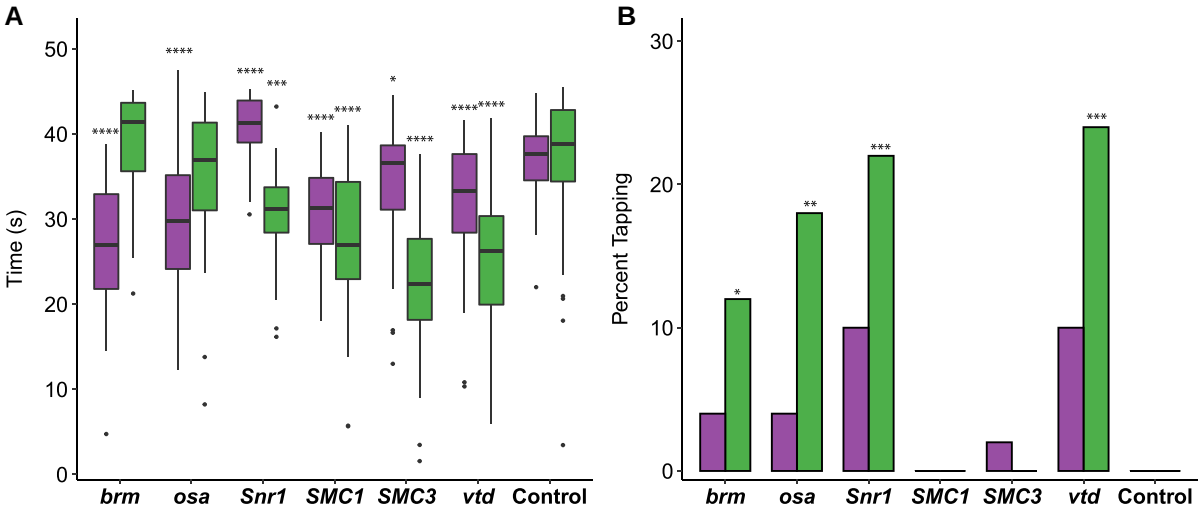

Fig. 1. Altered startle response phenotypes in SSRIDD and CdLS fly models. Startle phenotypes of flies with *Ubi156-GAL4*-mediated RNAi knockdown. a) Boxplots showing the time, in seconds, spent moving after an initial startle force. Asterisks represent sex-specific pairwise comparisons with the control. b) Bar graphs showing the percentage of flies that exhibit tapping behavior (see Supplementary Files 1 and 2) following an initial startle stimulus. Female values are shown on the left of each bar and males on the right, respectively. See Supplementary Table 4 for ANOVAs (a) and Fisher's exact tests (b). $N = 36$–50 flies per sex per line. $^{*}P < 0.05$, $^{**}P < 0.01$, $^{***}P < 0.001$, $^{****}P < 0.0001$.

differentially expressed genes based on the significance of the line term. The numbers of differentially expressed genes used in GO enrichment gave maximal GO enrichment with minimal redundancy compared to other numbers of differentially expressed genes.

We performed k-means clustering (average linkage algorithm), sexes separately, on Ge-TMM normalized least squares means of 533 genes that had the highest Log2 fold-change (FC) in expression. We identified the cutoff threshold value for Log2FC by first sorting genes in descending order of maximal absolute value of Log2FC, then fitted lines to roughly linear segments of the generated distribution and designated the cutoff threshold as the Log2FC value of the index at the intersection of the two fitted lines. We used hierarchical clustering (average linkage algorithm, WPGMA) to determine the approximate number of natural clusters, then performed clustering with varying values of k to determine the largest number of unique, but not redundant, expression patterns. We also performed GO statistical over-representation analyses on genes in each k-means cluster (GO Ontology database released 2022 July 01, Pantherdb v17.0 (Mi *et al.* 2013; Thomas *et al.* 2022)) in each disease-specific and pairwise analysis for GO biological process, molecular function, and reactome pathway terms.

Results

Drosophila models of SSRIDDs and CdLS

We identified Drosophila orthologs of 12 human genes associated with the SSRIDD chromatin remodeling disorders and CdLS with a DIOPT score >9 and for which TRiP RNAi lines in a common genetic background and without predicted off-target effects were publicly available. Using these criteria, the Drosophila genes *Bap111*, *brm*, *osa*, and *Snr1* are models of SSRIDD-associated genes *ARID1A*, *ARID1B*, *SMARCA2*, *SMARCA4*, *SMARCB1*, and *SMARCE1*; and *Nipped-B*, *SMC1*, *SMC3*, and *vtd* are models of CdLS-associated genes *NIPBL*, *SMC1A*, *SMC3*, and *RAD21* (Supplementary Table 2).

We obtained *UAS*-RNAi lines generated in the same genetic background for each of the fly orthologs and crossed these RNAi lines to each of three ubiquitous *GAL4* drivers to assess viability (Supplementary Fig. 1). We selected ubiquitous drivers since the human SSRIDD- and CdLS-associated genes and Drosophila orthologs are ubiquitously expressed, and SSRIDD and CdLS patients carry pathogenic variants in all cells. We initially crossed each *UAS*-RNAi line to three ubiquitous *GAL4* drivers (*Actin-GAL4*, *Ubiquitin-GAL4*, and *Ubi156-GAL4*) and assessed viability and degree of gene knockdown in the F1 progeny

(Supplementary Fig. 1). *Ubiquitin-GAL4*-mediated gene knockdown resulted in viable progeny in only three of the eleven *UAS-RNAi* lines, with most progeny dying during the embryonic or larval stage (Supplementary Fig. 1). Based on these data, we selected the weak ubiquitin driver *Ubi156-GAL4* (Garlapow *et al.* 2015) and the *UAS-RNAi* lines for *brm*, *osa*, *Snr1*, *SMC1*, *SMC3*, and *vtd* for further study (Table 1). With the exception of *Ubi156 > osa* males which had ~15% gene knockdown, RNAi knockdown of all genes ranged from 40–80% (Supplementary Table 3). Given that SSRIDDs and CdLS are largely autosomal dominant disorders, knockdown models that retain some degree of gene expression are reflective of the genetic landscape of SSRIDD and CdLS patients.

Effects on startle response

Given the neurological and musculoskeletal clinical findings in SSRIDD, and CdLS patients (Schrier Vergano *et al.* 2013; Bogershausen and Wollnik 2018; Kline *et al.* 2018; Avagliano *et al.* 2020; Selicorni *et al.* 2021; Vasko and Schrier Vergano 2022), we assessed startle-induced sensorimotor integration for RNAi of *brm*, *osa*, *Snr1*, *SMC1*, *SMC3*, and *vtd* relative to their control genotype. Almost all genotypes exhibited a decreased startle response across both sexes ($P < 0.02$ for all by-sex by-genotype comparisons to the control, Fig. 1a, Supplementary Table 4). Males with *osa* or *brm* knockdown did not exhibit changes in startle response ($P > 0.05$), and females with *Snr1* knockdown showed an increased startle response ($P < 0.0001$). In the lines where both sexes were affected, we observed more extreme phenotypes in males (Fig. 1a).

While testing flies for startle response, we noticed that some flies exhibited a specific locomotion phenotype we termed "tapping". Tapping is characterized by repetitive extension and retraction of individual legs as if to walk, but without progressive movement in any direction (Supplementary File 1). Compared to the control (example shown in Supplementary File 2), we observed an increase in the number of flies exhibiting tapping behavior in male flies with knockdown of *brm* ($P = 0.0267$), *osa* ($P = 0.0026$), *Snr1* ($P = 0.0005$) and *vtd* ($P = 0.0002$) (Fig. 1b, Supplementary Table 4). We also observed increases in tapping behavior in females with knockdown of *Snr1* and *vtd* that fall just outside of a significance level of 0.05 ($P = 0.0563$ for both genes); Fig. 1b, Supplementary Table 4). The tapping and startle phenotypes were not evident across all genes associated with a specific disorder.

Effects on sleep and activity

We hypothesized that hypotonia and sleep disturbances observed in SSRIDD and CdLS patients (Liu and Krantz 2009; Stavinoha *et al.* 2010; Rajan *et al.* 2012; Schrier Vergano *et al.* 2013; Zambrelli *et al.* 2016; Bogenshausen and Wollnik 2018; Vasko *et al.* 2021) may correspond to changes in activity and sleep in Drosophila models. Sleep disturbances were also observed in a previous Drosophila model of *NIPBL*-CdLS (Wu *et al.* 2015). Therefore, we quantified activity and sleep phenotypes for RNAi-mediated knockdown of *brm*, *osa*, *Snr1*, *SMC1*, *SMC3*, and *vtd*. All RNAi genotypes showed increases in overall spontaneous locomotor activity ($P < 0.02$ for all by-sex by-genotype comparisons to the control, Fig. 2a, Supplementary Table 4). This increase in spontaneous locomotor activity was most pronounced in males with knockdown of *osa* ($P < 0.0001$); this was the only genotype for which males were more active than females (Fig. 2a, Supplementary Table 4). All RNAi genotypes showed decreases in night sleep ($P < 0.0001$ for all by-sex by-genotype comparisons to the control). Flies with knockdown of *osa* (males, $P < 0.0001$; females, $P < 0.0001$) and females with knockdown of *vtd* ($P < 0.0001$) spent about half of the nighttime awake, the least amount of sleep across all flies tested (Fig. 2b, Supplementary Table 4). In addition to increased activity, the Drosophila models of SSRIDDs and CdLS have fragmented sleep: the number of sleep bouts at night was increased for all lines and sexes compared to the control ($P < 0.0001$ for all by-sex by-genotype comparisons to the control, except *SMC1* males, $P = 0.0023$, Fig. 2c, Supplementary Table 4).

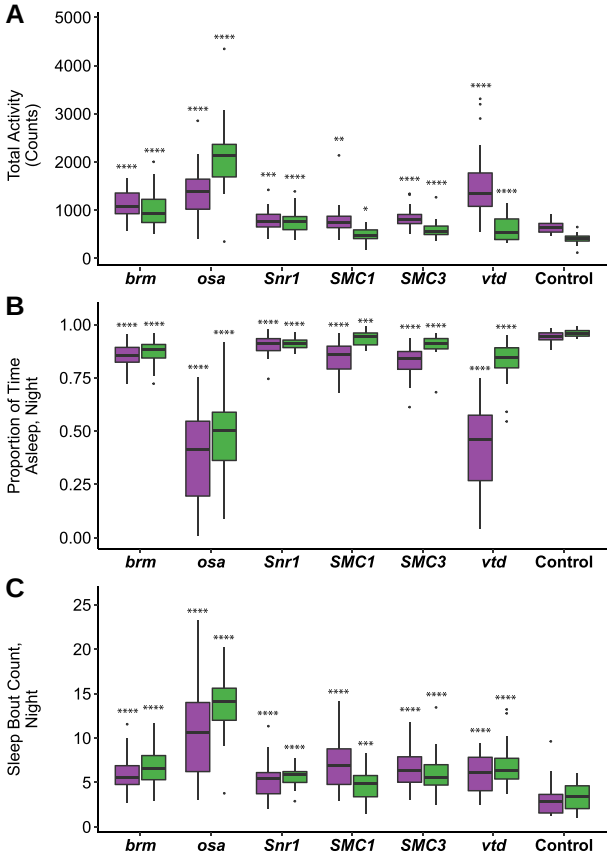

Fig. 2. Altered sleep and activity phenotypes in SSRIDD and CdLS fly models. Boxplots displaying activity and sleep phenotypes of flies with *Ubi156-GAL4*-mediated RNAi knockdown. a) total activity; b) proportion of time spent asleep at night; c) a number of sleep bouts at night. Females and males are shown on the left and right for each gene's box plot, respectively. $N = 18–32$ flies per sex per line. See Supplementary Table 4 for ANOVAs. Asterisks indicate pairwise comparisons of each line to the control, sexes separately. $^{*}P < 0.05$, $^{**}P < 0.01$, $^{***}P < 0.001$, $^{****}P < 0.0001$.

Effects on brain morphology

To assess changes in brain structure in *brm*, *osa*, *Snr1*, *SMC1*, *SMC3*, and *vtd* RNAi genotypes, we focused on the mushroom body and the ellipsoid body, as prior studies on SSRIDDs in flies have shown changes in a mushroom body structure (Chubak *et al.* 2019), and the mushroom body has been linked with regulation of sleep and activity in Drosophila (Joiner *et al.* 2006; Pitman *et al.* 2006; Guo *et al.* 2011; Sitaraman *et al.* 2015). Furthermore, SSRIDD and CdLS patients often present with intellectual disability and CNS abnormalities (Schrier Vergano *et al.* 2013; Bogershausen and Wollnik 2018; Kline *et al.* 2018; Avagliano *et al.* 2020; Selicorni *et al.* 2021; Vasko and Schrier Vergano 2022). In the Drosophila brain, the mushroom body mediates experience-dependent modulation of behavior (reviewed in Modi *et al.* 2020), making

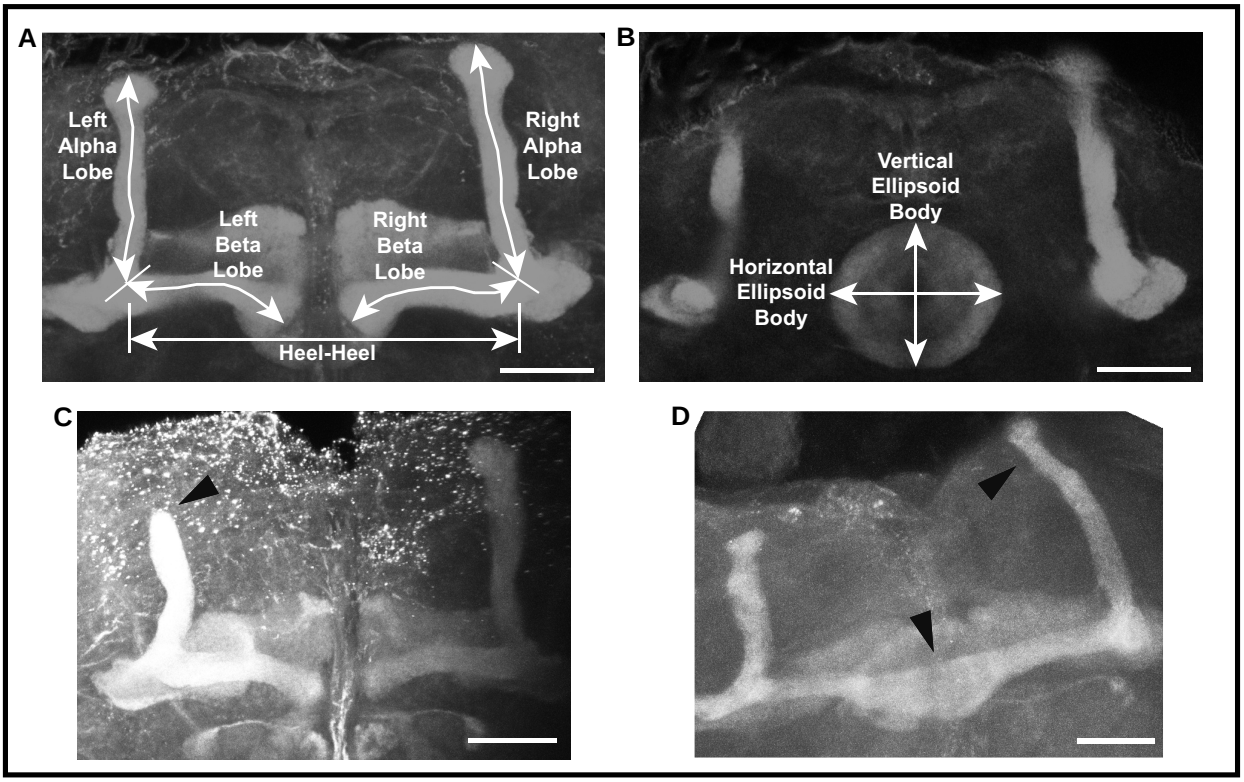

Fig. 3. Examples of mushroom body abnormalities in SSRIDD and CdLS fly models. Images of a wild type mushroom body annotated with measurement descriptors for (a) mushroom body alpha and beta lobes, and heel-heel normalization measurement; and b) ellipsoid body measurements. Images of select brains from flies with *Ubi156-GAL4*-mediated RNAi knockdown of *osa* showing (c) stunted alpha lobe outgrowth and narrowed alpha lobe head in a female *osa*-deficient fly brain; and d) beta lobe crossing the midline/fused beta lobes, as well as a skinny alpha lobe in a male *osa*-deficient fly brain. Images shown are z-stack maximum projections from confocal imaging. Triangular arrowheads indicate the abnormalities. The scale bar represents 25 μM.

the mushroom body and the ellipsoid body, which mediates sensory integration with locomotor activity, suitable targets for examining changes in brain structure. We used confocal microscopy to quantify the lengths of both alpha and beta lobes of the mushroom body, as well as the horizontal and vertical lengths of the ellipsoid body (Fig. 3a and b). The lengths of these lobes were measured in three dimensions, capturing the natural curvature of the alpha and beta lobes of the mushroom body instead of relying upon a 2D measurement of a 3D object.

We observed sex-specific changes in brain morphology (Fig. 3c and d). Females, but not males, showed decreased ellipsoid body dimensions with knockdown of *Snr1* (horizontal, $P = 0.0002$; vertical, $P < 0.0444$, Supplementary Table 4), while knockdown of *vtd* in females showed decreased alpha ($P = 0.0088$) and beta ($P = 0.0433$) lobe lengths. In addition to sex-specific effects, we observed sexually dimorphic effects; females with knockdown of *brm* showed decreases in alpha lobe and horizontal ellipsoid body length ($P = 0.0409$, $P = 0.0224$, respectively), while *brm* knockdown males showed increases in alpha lobe and horizontal ellipsoid body length ($P = 0.0301$, $P = 0.0305$, respectively; Fig. 4, Supplementary Table 4). Levene's tests for equality of variances indicate that the ellipsoid body measurements have sex-specific unequal environmental variances in some genotypes compared to the control (Fig. 4, Supplementary Table 4). These results show that these models of SSRIDDs and CdLS show morphological changes in the mushroom body and ellipsoid body.

We also recorded gross morphological abnormalities, such as missing lobes, beta lobes crossing the midline, and impaired/abnormal alpha lobe outgrowth (Fig. 3c and d). Although each abnormality was observed across multiple genotypes, only flies with knockdown of *osa* demonstrated consistent brain abnormalities. Male and female *osa* knockdown flies both exhibited an increased number of alpha lobes with impaired outgrowth (males: $P < 0.0001$, females: $P < 0.0025$, Fig. 4e, Supplementary Table 4), and the *osa* knockdown males also showed a significant number of beta lobe midline defects ($P = 0.0471$, Fig. 4f, Supplementary Table 4). Males with knockdown of *SMC1* and *vtd* also showed increased numbers of abnormal brains ($P = 0.0471$, $P = 0.0202$, respectively; Fig. 4g, Supplementary Table 4). Changes in brain morphology are more gene- and sex-dependent than changes in sleep, activity, and startle response.

Effects on genome-wide gene expression

We performed a genome-wide analysis of gene expression for the *brm*, *osa*, *Snr1*, *SMC1*, *SMC3*, and *vtd* RNAi genotypes and their control, separately for males and females. We first performed a factorial fixed effects analysis of variance (ANOVA) for each expressed transcript, partitioning variance in gene expression between sexes, lines, and the line-by-sex interaction for all seven genotypes. We found that 8,481 and 6,490 genes were differentially expressed (FDR < 0.05 for the line and/or line × sex terms, Supplementary Table 5), for a total of 9,657 unique genes.

brm, *osa*, *Snr1*, and their human orthologs (Tables 1, Supplementary Table 2) are part of the same protein complex (BAF complex in humans, BAP complex in flies). Therefore, we evaluated whether other BAP complex members *Bap55*, *Bap60*, and *Bap111* (which are orthologous to human BAF complex members *ACTL6A*, *SMARCD1*, and *SMARCE1*, respectively), are differentially expressed in the analysis of all genes. We observed differential expression of strong fly orthologs (DIOPT > 9) of

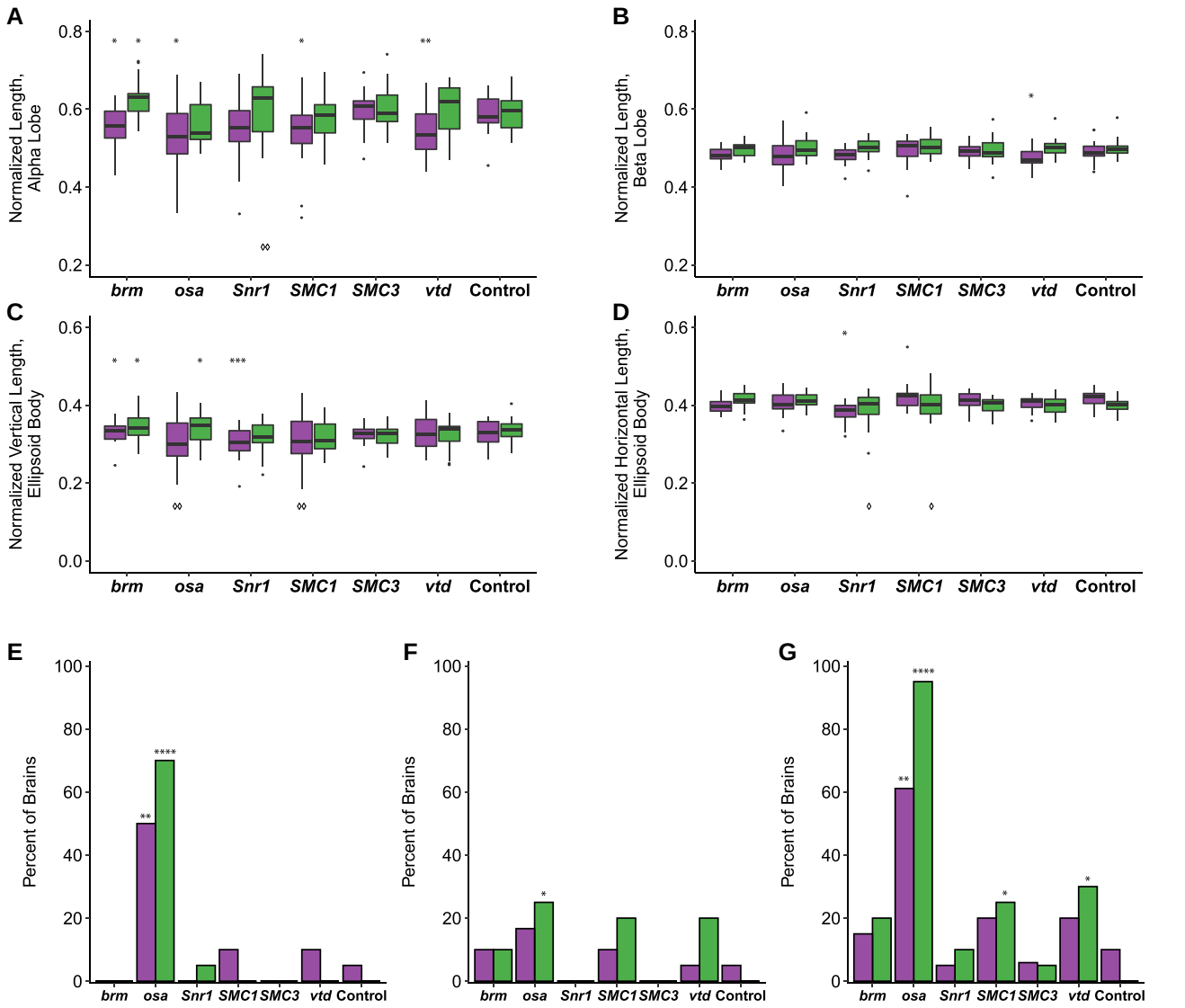

Fig. 4. SSRIDD and CdLS fly models show gene-specific changes in the mushroom body and ellipsoid body. Boxplots showing (a) the average alpha lobe and (b) beta lobe length for each brain; c) ellipsoid body height (vertical direction; dorsal-ventral) and (d) width (left-right; lateral). Bar graphs showing the percentage of brains that (e) have a stunted alpha lobe(s)/narrowed alpha lobe head(s); f) have a beta lobe(s) crossing the midline, including fused beta lobes; and (g) display one of more of the following defects: skinny alpha lobe, missing alpha lobe, skinny beta lobe, missing beta lobe, stunted alpha lobe/narrowed alpha lobe head, beta lobe crossing the midline/fused beta lobes, extra projections off of the alpha lobe, extra projections off of the beta lobe. See Fig. 3. All brains were dissected from flies with *Ubi156-GAL4*-mediated RNAi knockdown. For panels a-d, brains missing only one alpha or beta lobe are represented by the length of the remaining lobe, and brains missing both alpha lobes or both beta lobes were not included in the analyses. For panels e-g, data were analyzed with a Fisher's exact test, sexes separately. Asterisks (*) and diamonds (panels a-d only; ◊) represent pairwise comparisons of the knockdown line vs the control in ANOVAs or Fisher's Exact tests, and Levene's tests for unequal variances, respectively. See Supplementary Table 4 for ANOVAs, Fisher's exact and Levene's test results. Females and males are shown on the left and right box plots for each gene, respectively. $N = 17–20$ brains per sex per line. *$P < 0.05$, **$P < 0.01$, ***$P < 0.001$, ****$P < 0.0001$. ◊$P < 0.05$, ◊◊$P < 0.01$.

additional BAF complex subunits in the global model and found that *Bap55* and *Bap60* (FDR-corrected Line *P*-values: 0.0123, 0.01306, respectively; Supplementary Table 5), but not *Bap111*, are differentially expressed. We did not observe differential expression of *Nipped-B* in the global analysis. *Nipped-B* is a member of the fly cohesin complex along with *SMC1*, *SMC3*, and *vtd*, and is orthologous to the human cohesin complex member *NIPBL*.

We next performed separate pairwise analyses for SSRIDD-associated fly orthologs and CdLS-associated fly orthologs against the control genotype using the subset of 9,657 unique differentially expressed genes from the full ANOVA model (Tables 2, Supplementary Table 5). We also performed these analyses on sexes separately (Tables 2, Supplementary Table 5). The number of differentially expressed genes at a given FDR threshold varies across pairwise comparisons and across sexes. For example, females with knockdown of *brm* and *Snr1* have 583 and 3,026 differentially expressed genes (FDR < 0.05), respectively, whereas males with knockdown of these genes have 2,996 and 3,376 differentially expressed genes (FDR < 0.05), respectively (Tables 2, Supplementary Table 5). We observed the largest number of differentially expressed genes in flies with knockdown of *Snr1* (Tables 2, Supplementary Table 5). At FDR < 0.0005, there were still 1,059 genes differentially expressed in *Snr1* males (Supplementary Table 5). A greater number of differentially expressed genes are upregulated than downregulated in flies with knockdown of *brm*, *SMC1*, *SMC3*, and *vtd* (Supplementary

Table 2. Differentially expressed gene counts.

	Analysis			
	Both sexes		Females only	Males only
Comparison	Line	Line × Sex	Line	Line
brm vs Control	2,808	1,652	583	2,995
osa vs Control	2,179	1,059	1,135	1,580
Snr1 vs Control	4,996	3,632	3,026	3,376
SMC1 vs Control	2,714	1,727	2,540	2,395
SMC3 vs Control	1,874	586	2,711	1,161
vtd vs Control	1,998	961	818	1,630

The table shows the number of differentially expressed genes (FDR < 0.05) for the line and/or line × sex terms for each pairwise analysis of knockdown vs control, sexes together, and sexes separately.

Table 5). In contrast, flies with knockdown of *osa* and *Snr1* have a greater number of downregulated genes (Supplementary Table 5). Flies with knockdown of *Snr1* and *SMC1* had the greatest percentage of differentially expressed genes shared between males and females: 12.2% (698) and 7.6% (348), respectively (Supplementary Table 6). *Snr1* also had the greatest percent knockdown by RNAi. Only four genes are differentially expressed in all pairwise comparisons of knockdown lines vs the control line, in both males and females; all are computationally predicted genes (Supplementary Table 6).

We performed k-means clustering to examine patterns of co-regulated expression, separately for males ($k = 8$) and females ($k = 10$). We identified the cutoff threshold value for Log2FC by first sorting genes in descending order of the maximal absolute value of Log2FC (Supplementary Table 7). We fitted lines to roughly linear segments of the generated distribution and designated the cutoff threshold as the Log2FC value of the index at the intersection of the two fitted lines (Supplementary Fig. 2 and Supplementary Table 7). The genes in each cluster are listed in Supplementary Table 8. Although many clusters reveal gene-specific expression patterns (e.g. cluster F1, F9, F10, Fig. 5; clusters M1, M6, Fig. 6), clusters F7 and F8 show disease-specific patterns, where knockdown of *brm, osa,* and *Snr1* clusters separately from *SMC1*, *SMC3*, and *vtd* (Fig. 5). This is not surprising, as *brm, osa,* and *Snr1* are part of the fly BAF complex and models for SSRIDDs, whereas *SMC1*, *SMC3*, and *vtd* are associated with the fly cohesin complex and are models for CdLS. We also observed patterns involving genes from both SSRIDDs and CdLS. Clusters F4 and M3 contain genes upregulated in response to knockdown of *SMC3, osa,* and *brm* and downregulated in response to knockdown of *Snr1* and *SMC1* (Figs. 5 and 6) clusters F5 and M5 contain genes upregulated only in flies with knockdown of *osa* and *Snr1* (Figs. 5 and 6). Notably, many long noncoding RNAs (lncRNAs) feature prominently in many of the male and female clusters (Figs. 5 and 6; Supplementary Tables 7 and 8).

To infer the functions of these differentially expressed genes, we performed Gene Ontology (GO) analyses on the top approximately 600 (1000) differentially expressed genes for sexes separately (sexes pooled) (Supplementary Table 9). These analyses reveal that differentially expressed genes associated with the knockdown of CdLS-associated fly orthologs are involved in chromatin organization, regulation and processing of RNA, reproduction and mating behavior, peptidyl amino acid modification, and oxidoreductase activity (Supplementary Table 9). We also see sex-specific effects, such as muscle cell development in males and neural projection development in females (Supplementary Table 9). Differentially expressed genes associated with knockdown of SSRIDD-associated fly orthologs in males are involved in mating behavior, cilia development, and muscle contraction, while we see overrepresented ontology terms involved in chromatin modification, mitotic cell cycle, and serine hydrolase activity in females (Supplementary Table 9). We observed more alignment of GO terms across genes and sexes in the CdLS fly models (*SMC1*, *SMC3*, *vtd*) than in SSRIDD fly models (*brm*, *osa*, *Snr1*). There were no overrepresented GO terms for females in the CdLS-specific analysis. However, in the 156 genes shared across both sexes and both the SSRIDD and CdLS disease-level analyses, we see an over-representation of muscle cell development and actin assembly and organization (Supplementary Table 9). GO enrichment on k-means clusters does not reveal an over-representation of any biological processes, molecular functions, or pathways for clusters F7, F8, F4, F5, and M3 (Supplementary Table 10). Genes involved in alpha-glucosidase activity are overrepresented in Cluster M5 (Supplementary Table 10).

We generated Venn diagrams (Supplementary Fig. 3) to display the degree of similarity in differentially expressed genes across analyses, including the 156 genes shared across SSRIDD and CdLS males and females (Supplementary Table 6). Interestingly, 93% (2,689/2,907) of genes differentially expressed in a disease-specific analysis of CdLS males were also differentially expressed in CdLS females or in SSRIDD fly models (Supplementary Table 6). This is in contrast to CdLS females, SSRIDD males, and SSRIDD females, in which about 25% of the differentially expressed genes were specific to a single analysis (Supplementary Table 6). Approximately 24 and 56% of the differentially expressed genes (FDR < 0.05) in pairwise comparisons for males and females, respectively, have a predicted human ortholog (DIOPT > 9) (Supplementary Table 11).

Co-regulated genes

We selected a subset of co-regulated genes from gene expression analyses as potential modifiers of the focal genes *brm*, *osa*, and/or *Snr1*. We chose genes that had a significant effect (line FDR < 0.05) in analyses pooled across sexes, a suggestive effect (line FDR < 0.1) for each sex separately, a greater than or less than 2-fold-change in both sexes, a strong human ortholog (DIOPT > 9), and an available *attp40* TRiP RNAi line (the same genetic background as the focal genes). We increased the FDR threshold to 0.1 for the sex-specific pairwise analyses to account for the decreased power of these analyses compared to those with sexes combined. This resulted in 31 genes (Supplementary Table 12). We further narrowed our selection by prioritizing genes for further study with potential roles in neurological tissues, metabolism, chromatin, orthologs associated with disease in humans, and computationally predicted genes of unknown function. The six fly genes we selected for further study are *Alp10*, *CG40485*, *CG5877*, *IntS12*, *Mal-A4*, and *Odc1*, which are orthologous to human genes *ALPG*, *DHRS11*, *NRDE2*, *INTS12*, *SLC3A1*, and *ODC1*, respectively (human ortholog with highest DIOPT score listed; Supplementary Table 12). All six genes tested were co-regulated with *Snr1*, but *CG40485* and *CG5877* were not co-regulated with *osa* and *brm* models of SSRIDDs (Supplementary Table 6).

For each target gene, we crossed the *UAS-RNAi* line to the *Ubi156-GAL4* driver and performed qRT-PCR to assess the magnitude of reduction in gene expression. All co-regulated genes had reduced expression in both sexes (Supplementary Table 13). We then assessed the effects of these genes on startle response, sleep, and activity. Knockdown of *Mal-A4*, *CG5877*, and *Alp10* showed changes in startle response times for both sexes (Supplementary Fig. 4a, Supplementary Table 14). *Mal-A4* demonstrated sexually dimorphic changes in startle response similar to flies with *Snr1*

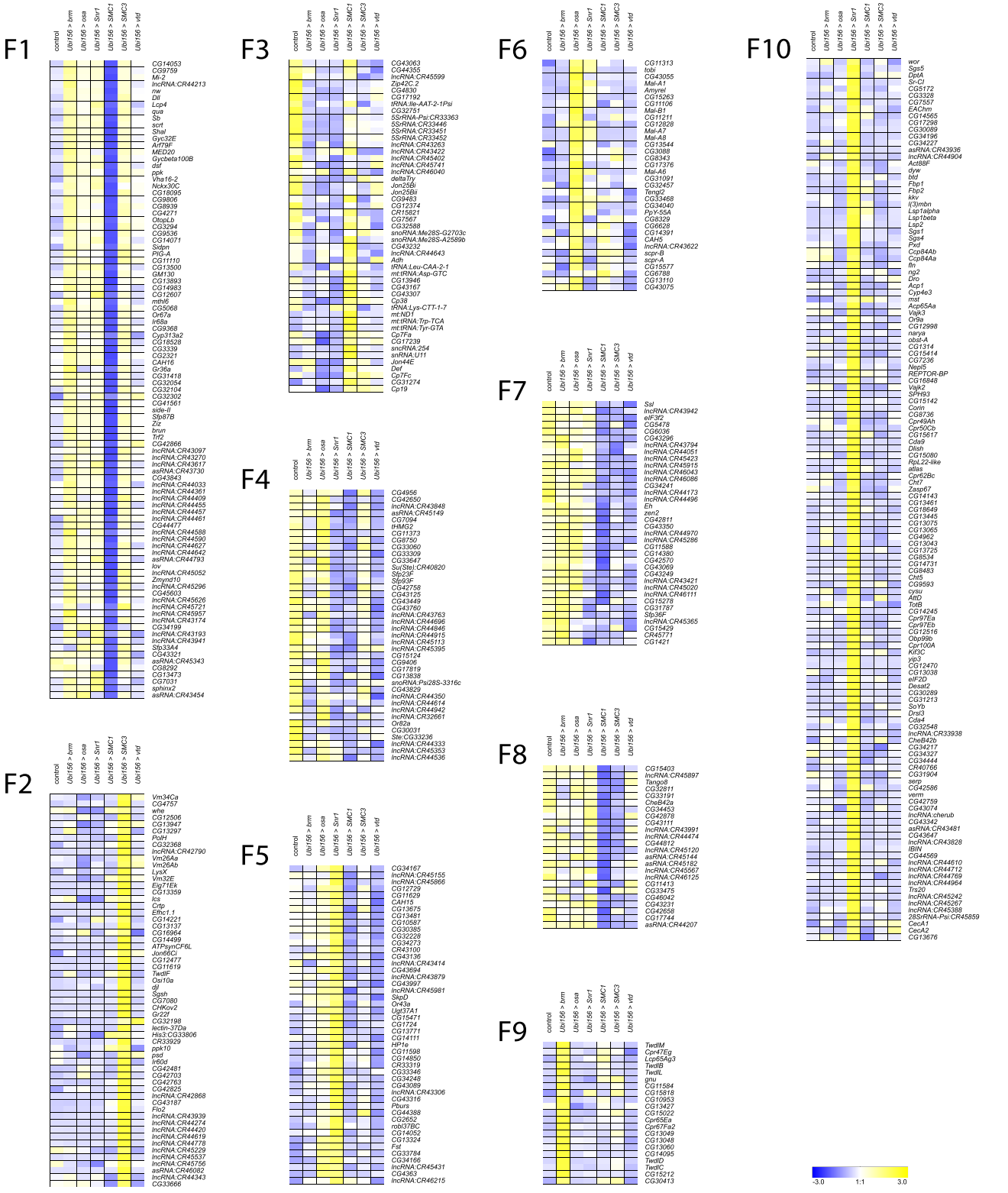

Fig. 5. *k*-means clusters for females. *k*-means clusters ($k = 10$, average linkage algorithm) based on expression patterns of the 535 genes with the maximal absolute value of the fold-change in expression, compared to the control. Blue and yellow indicate lower and higher expression, respectively.

knockdown, as females showed an increase ($P = 0.0215$) and males showed a decrease ($P < 0.0001$) in startle response (Supplementary Fig. 4a, Supplementary Table 14). We also quantified tapping behavior in these co-regulated genes and found that flies with knockdown of *CG5877* and *Odc1* showed an increase in tapping behavior compared to the control, similar to flies with knockdown of *osa* and *Snr1* (Fig. 1b), although we only observed tapping in females with knockdown of *Odc1* (Supplementary Fig. 4b, Supplementary Table 14; *CG5877* females: $P = 0.0266$, *CG5877* males: $P < 0.0001$; *Odc1* females: $P = 0.0125$).

With the exception of *CG40485*, which showed no changes in sleep or activity for either sex, all male RNAi genotypes had

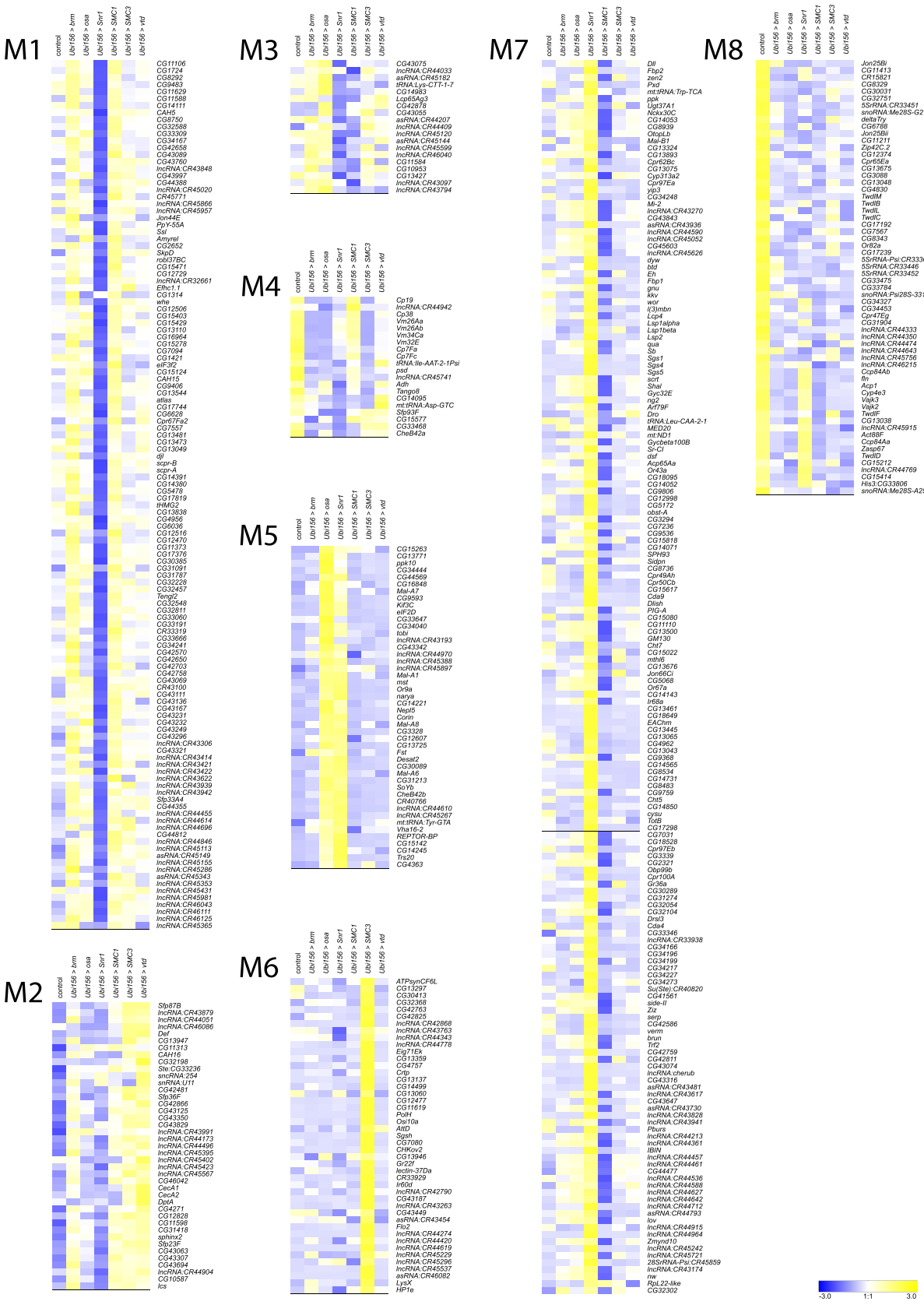

Fig. 6. *k*-means clusters for males. *k*-means clusters ($k = 8$, average linkage algorithm) based on expression patterns of the 535 genes with the maximal absolute value of the fold-change in expression, compared to the control. Blue and yellow indicate lower and higher expression, respectively.

increased nighttime sleep bouts ($P < 0.03$), decreased night sleep ($P < 0.03$), and, with the additional exception of *CG5877* RNAi flies, increased overall activity ($P < 0.006$) (Supplementary Fig. 4, Supplementary Table 14). Knockdown of *Mal-A4* and *Odc1* also showed increased activity for females ($P = 0.0049$, $P = 0.0044$, respectively). Only knockdown of *CG5877* resulted in increased night sleep for females ($P = 0.0014$) (Supplementary Fig. 4c and d, Supplementary Table 14). These changes in activity and sleep phenotype largely parallel those observed for SSRIDD fly models (Fig. 2, Supplementary Table 14).

Based on effects on startle response, tapping behavior, locomotor activity, night sleep, and sleep bouts, none of the phenotypes associated with RNAi of the co-regulated genes exactly matched the phenotypes associated with RNAi of the SSRIDD focal genes in both magnitude and direction. However, three genes (*Mal-A4*, *CG5877*, and *Odc1*) exhibited at least one altered phenotype in both sexes (Supplementary Fig. 4). These phenotypic observations suggest that *Mal-A4*, *CG5877*, and/or *Odc1* may be interacting with the focal genes of the SSRIDD fly models.

Discussion

Variants in members of the mammalian SWI/SNF complex (BAF complex) give rise to SSRIDDs, Mendelian disorders with a wide range of phenotypic manifestations, including Coffin–Siris and Nicolaides–Baraitser syndromes (reviewed in Schrier Vergano *et al.* 2013; Bogershausen and Wollnik 2018). The diverse consequences of such variants and variation in the penetrance of similar variants in different affected individuals suggest the presence of segregating genetic modifiers. Such modifiers may represent targets for ameliorating therapies or serve as indicators of disease severity, yet they cannot be easily identified in humans due to the limited sample size of individuals with rare disorders. In addition to identifying potential modifiers, Drosophila models can be used to understand the underlying molecular effects of variants in chromatin-modification pathways and may aid in the discovery of drugs that ameliorate deleterious phenotypic effects.

We used a systematic comparative genomics approach to generate Drosophila models of disorders of chromatin modification, based on the assumption that fundamental elements of chromatin modification are evolutionarily conserved. First, we reduced the expression of BAF and cohesin complex orthologs through targeted RNA interference with a *GAL4* driver that induces minimal lethality. We assessed the consequences of target gene knockdown on behaviors that mimic those affected in patients with SSRIDDs and CdLS. We used startle behavior, a proxy for sensorimotor integration, and sleep and activity phenotypes to assess the effects of variants in fly orthologues of human genes associated with similar behavioral disorders. These Drosophila models show increased activity, decreased night sleep, and changes in sensorimotor integration. Although we cannot readily recapitulate cognitive developmental defects in Drosophila, these behavioral phenotypes along with brain morphology measurements provide a representative spectrum of behaviors that correlate with human disease phenotypes. We observed gene-specific effects. In addition to showing the largest changes in sleep and activity phenotypes, only *osa* RNAi flies showed stunted mushroom body alpha lobes. Furthermore, only females with knockdown of *Snr1* showed an increase in startle response times. Our neuroanatomical studies focused on morphological changes in the ellipsoid body and mushroom bodies. We cannot exclude effects on other regions in the brain.

Next, we performed whole genome transcriptional profiling to identify co-regulated genes with each focal gene and used stringent filters to identify candidate modifier genes from the larger subset of co-regulated genes. *k*-means clustering reveals co-regulated genes unique to the knockdown of a single protein complex member (Supplementary Figs. 4 and 5), yet also shows genes co-regulated in response to the knockdown of several, but not all, members of the fly cohesin and SWI/SNF complexes. Gene-specific and cross-disease effects are intriguing, since *brm*, *osa*, and *Snr1* are part of the fly SWI/SNF complex, and *SMC1*, *SMC3*, and *vtd* are part of the fly cohesin complex, yet have widespread gene-specific downstream effects on gene regulation. Upon knockdown of one protein complex member, we did not necessarily find changes in the gene expression of other members of the same complex. It is possible that a compensatory mechanism exists that maintains transcript levels of other fly SWI/SNF or cohesin complex members or the focal genes themselves (Dorsett 2009; Raab *et al.* 2017; Van der Vaart *et al.* 2020), such as with *Nipped-B* in a CdLS fly model (Wu *et al.* 2015). Furthermore, the abundance of lncRNAs co-regulated with focal genes (Supplementary Figs. 4 and 5, Supplementary Table 8) is intriguing given the association between lncRNAs, chromatin modification, and changes in gene expression in both flies and humans (Li *et al.* 2019; Statello *et al.* 2021).

Snr1 is part of the Brahma complex, a core component of the BAP complex, and is orthologous to *SMARCB1* (Supplementary Table 2). *Odc1*, which encodes ornithine decarboxylase, is orthologous to *ODC1* (Supplementary Table 12), which is associated with Bachmann-Bupp syndrome, a rare neurodevelopmental disorder with alopecia, developmental delay, and brain abnormalities (Prokop *et al.* 2021; Bupp *et al.* 2022). Ornithine decarboxylase is the rate-limiting step of polyamine synthesis, which provides critical substrates for cell proliferation and differentiation (reviewed in Wallace *et al.* 2003; Pegg 2016). Polyamines interact with nucleic acids and transcription factors to modulate gene expression (Watanabe *et al.* 1991; Hobbs and Gilmour 2000; Miller-Fleming *et al.* 2015; Maki *et al.* 2017). *CG5877* is predicted to mediate post-transcriptional gene silencing as part of the spliceosome (Herold *et al.* 2009) and is orthologous to human *NRDE2* (Supplementary Table 12). *Mal-A4* is predicted to be involved in carbohydrate metabolism (Inomata *et al.* 2019) and is orthologous to *SLC3A1* (Supplementary Table 12). We observed extensive sexual dimorphism in behavioral phenotypes and transcriptional profiles upon knockdown of SSRIDD- and CdLS-associated genes.

Although we are not aware of transcriptional profiles currently available for SSRIDD patients, RNA sequencing of postmortem neurons from CdLS patients has shown dysregulation of hundreds of neuronal genes (Weiss *et al.* 2021). RNA sequencing in a *Nipped-B*-mutation fly model of *NIPBL*-CdLS found differential expression of ~2,800 genes in the imaginal disc (FDR < 0.05) (Wu *et al.* 2015). Thus, we believe the number of differentially expressed genes upon gene knockdown reported herein is comparable to previous studies.

Data availability

All high-throughput sequencing data are deposited in GEO GSE213763.

Raw behavioral data, qPCR data, and coding scripts are available on GitHub at https://github.com/rebeccamacpherson/Dmel_models_CSS_NCBRS_CdLS. All *UAS*-RNAi lines used in this study are available at the Bloomington Drosophila Stock Center,

except the ubiquitous RNAi driver *Ubi156-GAL4* and the double RNAi lines, which are available upon request.

Supplemental material available at GENETICS online.

Acknowledgements

We thank Dr. Lakshmi Sunkara for assistance with RNA sequencing, Marion R. Campbell III, Miller Barksdale, and Rachel C. Hannah for technical assistance with behavioral assays and brain dissections. We thank Dr. Joshua Walters for helping create Fig. 3 and helping dissect brains, and Dr. Richard Steet at the Greenwood Genetic Center for suggestions. We thank Katelynne Collins and Tori Gyorey for assistance with the RNAi studies. We thank the TRiP at Harvard Medical School (NIH/NIGMS R01-GM084947) for providing transgenic RNAi fly stocks used in this study.

Funding

This work was funded by NIH grants R01 GM128974 and P20 GM139769 to TFCM and RRHA, and F31 HD106719 to RAM.

Conflicts of interest

The author(s) declare no conflict of interest.

Author contributions

R.A.M. performed all experiments. V.S. assisted with RNA sequencing analysis; T.F.C.M. conceptualized the research program and T.F.C.M. and R.R.H.A. directed the research program. T.F.C.M., R.R.H.A., and R.A.M. provided resources and wrote the manuscript.

Literature Cited

Aoi H, Mizuguchi T, Ceroni JR, Kim VEH, Furquim I, Honjo RS, Iwaki T, Suzuki T, Sekiguchi F, Uchiyama Y, *et al.* Comprehensive genetic analysis of 57 families with clinically suspected Cornelia de Lange syndrome. J Hum Genet. 2019;64(10):967–978. doi:10.1038/s10038-019-0643-z.

Avagliano L, Parenti I, Grazioli P, Di Fede E, Parodi C, Mariani M, Kaiser FJ, Selicorni A, Gervasini C, Massa V. Chromatinopathies: a focus on Cornelia de Lange syndrome. Clin Genet. 2020;97(1):3–11. doi:10.1111/cge.13674.

Bögershausen N, Wollnik B. Mutational landscapes and phenotypic spectrum of SWI/SNF-related intellectual disability disorders. Front Mol Neurosci. 2018;11:252. doi:10.3389/fnmol.2018.00252.

Boyle MI, Jespersgaard C, Nazaryan L, Bisgaard A, Tümer Z. A novel *RAD21* variant associated with intrafamilial phenotypic variation in Cornelia de Lange syndrome—review of the literature. Clin Genet. 2017;91(4):647–649. doi:10.1111/cge.12863.

Bramswig NC, Caluseriu O, Lüdecke H-, Bolduc FV, Noel NCL, Wieland T, Surowy HM, Christen H-, Engels H, Strom TM, *et al.* Heterozygosity for *ARID2* loss-of-function mutations in individuals with a Coffin–Siris syndrome-like phenotype. Hum Genet. 2017;136(3):297–305. doi:10.1007/s00439-017-1757-z.

Bupp C, Michale J, VanSickle E, Rajasekaran S, Bachmann AS. Bachmann-Bupp syndrome. In: Adam MP, Everman DB, Mirzaa GM, editors. GeneReviews ®. Seattle (WA): University of Washington, Seattle; 2022.

Bushnell B. BBMap. SOURCEFORGE. 2014.

Chen S, Huang T, Zhou Y, Han Y, Xu M, Gu J. AfterQC: automatic filtering, trimming, error removing and quality control for fastq data. BMC Bioinformatics. 2017;18(S3):80. doi:10.1186/s12859-017-1469-3.

Chubak MC, Nixon KCJ, Stone MH, Raun N, Rice SL, Sarikahya M, Jones SG, Lyons TA, Jakub TE, Mainland RLM, *et al.* Individual components of the SWI/SNF chromatin remodelling complex have distinct roles in memory neurons of the Drosophila mushroom body. Dis Model Mech. 2019;12(3):dmm037325. doi:10.1242/dmm.037325.

Cichewicz K, Hirsh J. ShinyR-DAM: a program analyzing Drosophila activity, sleep and circadian rhythms. Commun Biol. 2018;1:25. doi:10.1038/s42003-018-0031-9.

Cucco F, Sarogni P, Rossato S, Alpa M, Patimo A, Latorre A, Magnani C, Puisac B, Ramos FJ, Pié J, *et al.* Pathogenic variants in *EP300* and *ANKRD11* in patients with phenotypes overlapping Cornelia de Lange syndrome. Am J Med Genet A. 2020;182(7):1690–1696. doi:10.1002/ajmg.a.61611.

Deardorff MA, Bando M, Nakato R, Watrin E, Itoh T, Minamino M, Saitoh K, Komata M, Katou Y, Clark D, *et al. HDAC8* mutations in Cornelia de Lange syndrome affect the cohesin acetylation cycle. Nature. 2012;489(7415):313–317. doi:10.1038/nature11316.

Deardorff MA, Kaur M, Yaeger D, Rampuria A, Korolev S, Pie J, Gil-Rodríguez C, Arnedo M, Loeys B, Kline AD, *et al.* Mutations in cohesin complex members *SMC3* and *SMC1A* cause a mild variant of Cornelia de Lange syndrome with predominant mental retardation. Am J Hum Genet. 2007;80(3):485–494. doi:10.1038/nature11316.

de Chaumont F, Dallongeville S, Chenouard N, Hervé N, Pop S, Provoost T, Meas-Yedid V, Pankajakshan P, Lecomte T, Le Montagner Y, *et al.* Icy: an open bioimage informatics platform for extended reproducible research. Nat Methods. 2012;9(7):690–696. doi:10.1038/nmeth.2075.

De Rubeis S, He X, Goldberg AP, Poultney CS, Samocha K, Cicek AE, Kou Y, Liu L, Fromer M, Walker S, *et al.* Synaptic, transcriptional and chromatin genes disrupted in autism. Nature. 2014;515(7526):209–215. doi:10.1038/nature13772.

Dorsett D. Cohesin, gene expression and development: lessons from Drosophila. Chromosome Res. 2009;17(2):185–200. doi:10.1007/s10577-009-9022-5.

Fox J, Weisberg S, editors. An R Companion to Applied Regression. Third ed. Thousand Oaks, CA: Sage; 2019.

Garlapow M, Huang W, Yarboro M, Peterson K, Mackay T. Quantitative genetics of food intake in *Drosophila melanogaster*. PLoS One. 2015;10(9):e0138129. doi:10.1371/journal.pone.0138129.

Gazdagh G, Blyth M, Scurr I, Turnpenny PD, Mehta SG, Armstrong R, McEntagart M, Newbury-Ecob R, Tobias ES, Joss S. Extending the clinical and genetic spectrum of *ARID2* related intellectual disability. A case series of 7 patients. Eur J Med Genet. 2019;62(1):27–34. doi:10.1016/j.ejmg.2018.04.014.

Gil-Rodríguez MC, Deardorff MA, Ansari M, Tan CA, Parenti I, Baquero-Montoya C, Ousager LB, Puisac B, Hernández-Marcos M, Teresa-Rodrigo ME, *et al.* De novo heterozygous mutations in *SMC3* cause a range of Cornelia de Lange syndrome-overlapping phenotypes. Hum Mutat. 2015;36(4):454–462. doi:10.1002/humu.22761.

Guo F, Yi W, Zhou M, Guo A. Go signaling in mushroom bodies regulates sleep in Drosophila. Sleep. 2011;34(3):273–281. doi:10.1093/sleep/34.3.273.

Hempel A, Pagnamenta AT, Blyth M, Mansour S, McConnell V, Kou I, Ikegawa S, Tsurusaki Y, Matsumoto N, Lo-Castro A, *et al.* Deletions and de novo mutations of *SOX11* are associated with a neurodevelopmental disorder with features of Coffin–Siris

syndrome. J Med Genet. 2016;53(3):152–162. doi:10.1136/jmedgenet-2015-103393.

Herold N, Will CL, Wolf E, Kastner B, Urlaub H, Lührmann R. Conservation of the protein composition and electron microscopy structure of Drosophila melanogaster and human spliceosomal complexes. Mol Cell Biol. 2009;29(1):281–301. doi:10.1128/MCB.01415-08.

Hobbs CA, Gilmour SK. High levels of intracellular polyamines promote histone acetyltransferase activity resulting in chromatin hyperacetylation. J Cell Biochem. 2000;77(3):345–360. doi:10.1002/(SICI)1097-4644(20000601)77:3<345::AID-JCB1>3.0.CO;2-P.

Hoyer J, Ekici A, Endele S, Popp B, Zweier C, Wiesener A, Wohlleber E, Dufke A, Rossier E, Petsch C, *et al.* Haploinsufficiency of *ARID1B*, a member of the SWI/SNF-A chromatin-remodeling complex, is a frequent cause of intellectual disability. Am J Hum Genet. 2012;90(3):565–572. doi:10.1016/j.ajhg.2012.02.007.

Hu Y, Flockhart I, Vinayagam A, Bergwitz C, Berger B, Perrimon N, Mohr SE. An integrative approach to ortholog prediction for disease-focused and other functional studies. BMC Bioinformatics. 2011;12(1):357. doi:10.1186/1471-2105-12-357.

Huggett SB, Hatfield JS, Walters JD, McGeary JE, Welsh JW, Mackay TFC, Anholt RRH, Palmer RHC. Ibrutinib as a potential therapeutic for cocaine use disorder. Transl Psychiatry. 2021;11(1):623. doi:10.1038/s41398-021-01737-5.

Huisman S, Mulder PA, Redeker E, Bader I, Bisgaard A, Brooks A, Cereda A, Cinca C, Clark D, Cormier-Daire V, *et al.* Phenotypes and genotypes in individuals with *SMC1A* variants. Am J Med Genet A. 2017;173A(8):2108–2125. doi:10.1002/ajmg.a.38279.

Inomata N, Takahasi KR, Koga N. Association between duplicated maltase genes and the transcriptional regulation for the carbohydrate changes in *Drosophila melanogaster*. Gene. 2019;686:141–145. doi:10.1016/j.gene.2018.11.007.

Iossifov I, O'Roak BJ, Sanders SJ, Ronemus M, Krumm N, Levy D, Stessman HA, Witherspoon KT, Vives L, Patterson KE, *et al.* The contribution of de novo coding mutations to autism spectrum disorder. Nature. 2014;515(7526):216–221. doi:10.1038/nature13908.

Jansen S, Kleefstra T, Willemsen MH, de Vries P, Pfundt R, Hehir-Kwa JY, Gilissen C, Veltman JA, de Vries BBA, Vissers LELM. De novo loss-of-function mutations in X-linked *SMC1A* cause severe ID and therapy-resistant epilepsy in females: expanding the phenotypic spectrum. Clin Genet. 2016;90(5):413–419. doi:10.1111/cge.12729.

Joiner WJ, Crocker A, White BH, Sehgal A. Sleep in Drosophila is regulated by adult mushroom bodies. Nature. 2006;441(7094):757–760. doi:10.1038/nature04811.

Kline AD, Moss JF, Selicorni A, Bisgaard A, Deardorff MA, Gillett PM, Ishman SL, Kerr LM, Levin AV, Mulder PA, *et al.* Diagnosis and management of Cornelia de Lange syndrome: first international consensus statement. Nat Rev Genet. 2018;19(10):649–666. doi:10.1038/s41576-018-0031-0.

Krantz ID, McCallum J, DeScipio C, Kaur M, Gillis LA, Yaeger D, Jukofsky L, Wasserman N, Bottani A, Morris CA, *et al.* Cornelia de Lange syndrome is caused by mutations in *NIPBL*, the human homolog of *Drosophila melanogaster Nipped-B*. Nat Genet. 2004;36(6):631–635. doi:10.1038/ng1364.

Li K, Tian Y, Yuan Y, Fan X, Yang M, He Z, Yang D. Insights into the functions of lncRNAs in Drosophila. Int J Mol Sci. 2019;20(18):4646. doi:10.3390/ijms20184646.

Liao Y, Smyth GK, Shi W. The subread aligner: fast, accurate and scalable read mapping by seed-and-vote. Nucleic Acids Res. 2013;41(10):e108. doi:10.1093/nar/gkt214.

Liu J, Krantz ID. Cornelia de Lange syndrome, cohesin, and beyond. Clin Genet. 2009;76(4):303–314. doi:10.1111/j.1399-0004.2009.01271.x.

Livak KJ, Schmittgen TD. Analysis of relative gene expression data using real-time quantitative PCR and the 2(−Δ Δ C(T)) method. Methods. 2001;25(4):402–408. doi:10.1006/meth.2001.1262.

Machol K, Rousseau J, Ehresmann S, Garcia T, Nguyen TTM, Spillmann RC, Sullivan JA, Shashi V, Yh J, Stong N, *et al.* Expanding the spectrum of BAF-related disorders: De novo variants in *SMARCC2* cause a syndrome with intellectual disability and developmental delay. Am J Hum Genet. 2019;104(1):164–178. doi:10.1016/j.ajhg.2018.11.007.

Maki K, Shibata T, Kawabata S. Transglutaminase-catalyzed incorporation of polyamines masks the DNA-binding region of the transcription factor relish. J Biol Chem. 2017;292(15):6369–6380. doi:10.1074/jbc.M117.779579.

Mi H, Muruganujan A, Thomas PD. PANTHER In 2013: modeling the evolution of gene function, and other gene attributes, in the context of phylogenetic trees. Nucleic Acids Res. 2013;41(D1):D377–D386. doi:10.1093/nar/gks1118.

Miller-Fleming L, Olin-Sandoval V, Campbell K, Ralser M. Remaining mysteries of molecular biology: the role of polyamines in the cell. J Mol Biol. 2015;427(21):3389–3406. doi:10.1016/j.jmb.2015.06.020.

Modi MN, Shuai Y, Turner GC. The Drosophila mushroom body: from architecture to algorithm in a learning circuit. Annu Rev Neurosci. 2020;43(1):465–484. doi:10.1146/annurev-neuro-080317-0621333.

Olley G, Ansari M, Bengani H, Grimes GR, Rhodes J, von Kriegsheim A, Blatnik A, Stewart FJ, Wakeling E, Carroll N, *et al. BRD4* Interacts with *NIPBL* and *BRD4* is mutated in a Cornelia de Lange-like syndrome. Nat Genet. 2018;50(3):329–332. doi:10.1038/s41588-018-0042-y.

Parenti I, Teresa-Roigo ME, Pozojevic J, Gil SR, Bader I, Braunholz D, Bramswig NC, Gervasini C, Larizza L, Pfeiffer L, *et al.* Mutations in chromatin regulators functionally link Cornelia de Lange syndrome and clinically overlapping phenotypes. Hum Genet. 2017;136(3):307–320. doi:10.1007/s00439-017-1758-y.

Pauli A, Althoff F, Oliveira RA, Heidmann S, Schuldiner O, Lehner CF, Dickson BJ, Nasmyth K. Cell-type-specific TEV protease cleavage reveals cohesin functions in Drosophila neurons. Dev Cell. 2008;14(2):239–251. doi:10.1016/j.devcel.2007.12.009.

Pegg AE. Functions of polyamines in mammals. J Biol Chem. 2016;291(29):14904–14912. doi:10.1074/jbc.R116.731661.

Perkins LA, Holderbaum L, Tao R, Hu Y, Sopko R, McCall K, Yang-Zhou D, Flockhart I, Binari R, Shim H, *et al.* The transgenic RNAi project at Harvard medical school: resources and validation. Genetics. 2015;201(3):843–852. doi:10.1534/genetics.115.180208.

Pitman J, McGill J, Keegan K, Allada R. A dynamic role for the mushroom bodies in promoting sleep in Drosophila. Nature. 2006;441-(7094):753–756. doi:10.1038/nature04739.

Prokop JW, Bupp CP, Frisch A, Bilinovich SM, Campbell DB, Vogt D, Schultz CR, Uhl KL, VanSickle E, Rajasekaran S, *et al.* Emerging role of *ODC1* in neurodevelopmental disorders and brain development. Genes (Basel). 2021;12(4):470. doi:10.3390/genes12040470.

Raab JR, Runge JS, Spear CC, Magnuson T. Co-regulation of transcription by BRG1 and BRM, two mutually exclusive SWI/SNF ATPase subunits. Epigenetics Chromatin. 2017;10(1):62. doi:10.1186/s13072-017-0167-8.

Rajan R, Benke JR, Kline AD, Levy HP, Kimball A, Mettel TL, Boss EF, Ishman SL. Insomnia in Cornelia de Lange syndrome. Int J Pediatr Otorhinolaryngol. 2012;76(7):972–975. doi:10.1016/j.ijporl.2012.03.008.

Santen G, Aten E, Sun Y, Almomani R, Gilissen C, Nielsen M, Kant SG, Snoeck IN, Peeters E, Hilhorst-Hofstee Y, *et al.* Mutations in SWI/SNF chromatin remodeling complex gene *ARID1B* cause Coffin-Siris syndrome. Nat Genet. 2012;44(4):379–380. doi:10.1038/ng.2217.

Schrier Vergano S, Santen G, Wieczorek D, Wollnik B, Matsumo N, Deardorff MA. Coffin-Siris syndrome. In: Adam MP, Everman DB, Mirzaa GM, *et al.*, editors. GeneReviews ®. Seattle (WA): University of Washington, Seattle; 2013.

Schuldiner O, Berdnik D, Levy JM, Wu JS, Luginbuhl D, Gontang AC, Luo L. piggyBac-based mosaic screen identifies a postmitotic function for cohesin in regulating developmental axon pruning. Dev Cell. 2008;14(2):227–238. doi:10.1016/j.devcel.2007.11.001.

Selicorni A, Mariani M, Lettieri A, Massa V. Cornelia de Lange syndrome: from a disease to a broader spectrum. Genes (Basel). 2021;12(7):1075. doi:10.3390/genes12071075.

Sitaraman D, Aso Y, Rubin GM, Nitabach MN. Control of sleep by dopaminergic inputs to the Drosophila mushroom body. Front Neural Circuits. 2015;9:73. doi:10.3389/fncir.2015.00073.

Smid M, Coebergh van den Braak R, van de Werken H, van Riet J, Galen A, Weerd V, Daane M, Bril S, Lalmahomed Z, Kloosterman WP, *et al.* Gene length corrected trimmed mean of M-values (GeTMM) processing of RNA-seq data performs similarly in intersample analyses while improving intrasample comparisons. BMC Bioinformatics. 2018;19(1):236. doi:10.1186/s12859-018-2246-7.

Statello L, Guo C, Chen L, Huarte M. Gene regulation by long noncoding RNAs and its biological functions. Nat Rev Mol Cell Biol. 2021;22(2):96–118. doi:10.1038/s41580-020-00315-9.

Stavinoha RC, Kline AD, Levy HP, Kimball A, Mettel TL, Ishman SL. Characterization of sleep disturbance in Cornelia de Lange syndrome. Int J Pediatr Otorhinolaryngol. 2010;75(2):215–218. doi:10.1016/j.ijporl.2010.11.003.

Symonds JD, Joss S, Metcalfe KA, Somarathi S, Cruden J, Devlin AM, Donaldson A, DiDonato N, Fitzpatrick D, Kaiser FJ, *et al.* Heterozygous truncation mutations of the *SMC1A* gene cause a severe early onset epilepsy with cluster seizures in females: detailed phenotyping of 10 new cases. Epilepsia. 2017;58(4):565–575. doi:10.1111/epi.13669.

Thomas PD, Ebert D, Muruganujan A, Mushayahama T, Albou L, Mi H. PANTHER: making genome-scale phylogenetics accessible to all. Protein Sci. 2022;31(1):8–22. doi:10.1002/pro.4218.

Tsurusaki Y, Koshimizu E, Ohashi H, Phadke S, Kou I, Shiina M, Suzuki T, Okamoto N, Imamura S, Yamashita M, *et al.* De novo *SOX11* mutations cause Coffin–Siris syndrome. Nat Commun. 2014;5(1):4011. doi:10.1038/ncomms5011.

Tsurusaki Y, Okamoto N, Fukushima Y, Homma T, Kato M, Hiraki Y, Yamagata T, Yano S, Mizuno S, Sakazume S, *et al.* Mutations affecting components of the SWI/SNF complex cause Coffin-Siris syndrome. Nat Genet. 2012;44(4):376–368. doi:10.1038/ng.2219.

van Allen MI, Filippi G, Siegel-Bartelt J, Yong S, McGillivray B, Zuker RM, Smith CR, Magee JF, Ritchie S, Toi A, *et al.* Clinical variability within Brachmann-de Lange syndrome: a proposed classification system. Am J Med Genet. 1993;47(7):947–958. doi:10.1002/ajmg.1320470704.

van der Sluijs PJ, Jansen S, Vergano SA, Adachi-Fukuda M, Alanay Y, AlKindy A, Baban A, Bayat A, Beck-Wödl S, Berry K, *et al.* The *ARID1B* spectrum in 143 patients: from nonsyndromic intellectual disability to Coffin–Siris syndrome. Genet Med. 2019;21(6):1295–1307. doi:10.1038/s41436-018-0330-z.

van der Vaart A, Godfrey M, Portegijs V, Heuvel S. Dose-dependent functions of SWI/SNF BAF in permitting and inhibiting cell proliferation in vivo. Sci Adv. 2020;6(21):eaay3823. doi:10.1126/sciadv.aay3823.

van Houdt JKJ, Nowakowska BA, Sousa SB, van Schaik BDC, Seuntjens E, Avonce N, Sifrim A, Abdul-Rahman OA, van den Boogaard MJ, Bottani A, *et al.* Heterozygous missense mutations in *SMARCA2* cause Nicolaides-Baraitser syndrome. Nat Genet. 2012;44(4):445–449. doi:10.1038/ng.1105.

Vasileiou G, Vergarajauregui S, Endele S, Popp B, Büttner C, Ekici AB, Gerard M, Bramswig NC, Albrecht B, Clayton-Smith J, *et al.* Mutations in the BAF-complex subunit *DPF2* are associated with Coffin-Siris syndrome. Am J Hum Genet. 2018;102(3):468–479. doi:10.1016/j.ajhg.2018.01.014.

Vasko A, Drivas TG, Schrier Vergano SA. Genotype-phenotype correlations in 208 individuals with Coffin-Siris syndrome. Genes (Basel). 2021;12(6):937. doi:10.3390/genes12060937.

Vasko A, Schrier Vergano SA. Language impairments in individuals with Coffin-Siris syndrome. Front Neurosci. 2022;15:802583. doi:10.3389/fnins.2021.802583.

Vissers LM, Gilissen C, Veltman JA. Genetic studies in intellectual disability and related disorders. Nat Rev Genet. 2016;17(1):9–18. doi:10.1038/nrg3999.

Wallace HM, Fraser AV, Hughes A. A perspective of polyamine metabolism. Biochem J. 2003;376(1):1–14. doi:10.1042/BJ20031327.

Watanabe S, Kusama-Eguchi K, Kobayashi H, Igarashi K. Estimation of polyamine binding to macromolecules and ATP in bovine lymphocytes and rat liver. J Biol Chem. 1991;266(31):20803–20809. doi:10.1016/S0021-9258(18)54780-3.

Weiss FD, Calderon L, Wang Y, Georgieva R, Guo Y, Cvetesic N, Kaur M, Dharmalingam G, Krantz ID, Lenhard B, *et al.* Neuronal genes deregulated in Cornelia de Lange syndrome respond to removal and re-expression of cohesin. Nat Commun. 2021;12(1):2919. doi:10.1038/s41467-021-23141-9.

Wu Y, Gause M, Xu D, Misulovin Z, Schaaf CA, Mosarla RC, Mannino E, Shannon M, Jones E, Shi M, *et al.* Drosophila *Nipped-B* mutants model Cornelia de Lange syndrome in growth and behavior. PLoS Genet. 2015;11(11):e1005655. doi:10.1371/journal.pgen.1005655.

Wu TD, Reeder J, Lawrence M, Becker G, Brauer MJ. GMAP and GSNAP for genomic sequence alignment: enhancements to speed, accuracy, and functionality. In: Mathé E, Davis S, editors. Statistical Genomics: Methods and Protocols. New York (NY): Springer New York; 2016. p. 283.

Yamamoto A, Zwarts L, Callaerts P, Norga K, Mackay TFC, Anholt RRH. Neurogenetic networks for startle-induced locomotion in *Drosophila melanogaster*. Proc Natl Acad Sci U S A. 2008;105(34):12393–12398. doi:10.1073/pnas.0804889105.

Zambrelli E, Fossati C, Turner K, Taiana M, Vignoli A, Gervasini C, Russo S, Furia F, Masciadri M, Ajmone P, *et al.* Sleep disorders in Cornelia de Lange syndrome. Am J Med Genet C. 2016;172(2):214–221. doi:10.1002/ajmg.c.31497.

Zawerton A, Yao B, Yeager JP, Pippucci T, Haseeb A, Smith JD, Wischmann L, Kühl SJ, Dean JCS, Pilz DT, *et al.* De novo *SOX4* variants cause a neurodevelopmental disease associated with mild dysmorphism. Am J Hum Genet. 2019;104(2):246–259. doi:10.1016/j.ajhg.2018.12.014.

Zirin J, Hu Y, Liu L, Yang-Zhou D, Colbeth R, Yan D, Ewen-Campen B, Tao R, Vogt E, VanNest S, *et al.* Large-scale transgenic Drosophila resource collections for loss- and gain-of-function studies. Genetics. 2020;214(4):755–767. doi:10.1534/genetics.119.302964.

Zwarts L, Vanden Broeck L, Cappuyns E, Ayroles JF, Magwire MM, Vulsteke V, Clements J, Mackay TFC, Callaerts P. The genetic basis of natural variation in mushroom body size in *Drosophila melanogaster*. Nat Commun. 2015;6(1):10115. doi:10.1038/ncomms10115.

Editor: H. Bellen